3D Hotspot Matrix of Au Nanoparticles on Au Nanostructures with a Spacer Layer of Dithiol Molecules for Highly Sensitive Surface-Enhanced Raman Spectroscopy

Dong-Jin Lee
Inha University
Dae Yu Kim (dyukim@inha.ac.kr)
Inha University

Research Article

Keywords: SERS, AuNP@BDMT@AuNSs, 3D Hotspot Matrix, Vertical Configuration with Nanogap, Spacer Layer of Dithiol Molecules, Pesticide Detection

Posted Date: July 30th, 2021

DOI: https://doi.org/10.21203/rs.3.rs-757278/v1

Abstract

Engineering of efficient plasmonic hotspots has been receiving great attention to enhance the sensitivity of surface-enhanced Raman scattering (SERS). In the present study, we propose a highly sensitive SERS platform based on Au nanoparticles (AuNPs) on Au nanostructures (AuNSs) with a spacer layer of 1,4-benzenedimethanethiol (BDMT). The three-dimensional (3D) hotspot matrix has been rationally designed based on the idea of employing 3D hotspots with a vertical nanogap between AuNSs and AuNPs after generating large area two-dimensional hotspots of AuNSs. AuNP@BDMT@AuNSs are fabricated by functionalizing BDMT on AuNSs and then immobilizing AuNPs. The Raman signal of the AuNP@BDMT@AuNSs is approximately twelve times higher than that of AuNSs at 100 nM of rhodamine 6G. The AuNP@BDMT@AuNSs are then employed to detect thiram, which is used as a fungicide, with a detection limit of 13 nM. Our proposed platform thus shows significant potential for use in highly sensitive SERS sensors.

1. Introduction

SERS has been extensively studied and widely adopted in a diverse range of applications, including chemical identification, biomedical diagnosis, and environmental, food, and industrial monitoring[1–6]. SERS substrates enhance the naturally weak Raman scattering signals of target analytes by employing plasmonic hotspots in metallic nanostructures (NSs) to boost and localize electromagnetic fields[1,7–9]. Traditionally, hotspot engineering has focused on the design of plasmonic building blocks, including materials and platforms with zero-dimensional to three-dimensional (3D) configurations[1,10–12]. Given the 3D laser excitation volume, 3D SERS platforms offer significant advantages over lower-dimensional SERS platforms. As such, various fabrication techniques have been proposed for the development of 3D SERS platforms, including top-down lithographic approaches and bottom-up self-assembly methods[6,8,13–21].

3D nanostructures created by molecule-based self-assembly have fascinated attention towards highly sensitive SERS platforms due to their cost-effective fabrication and ease of precise control of nanogap[22–27]. A variety of molecules have been utilized to assemble nanoparticles (NPs) into 3D configurations. For example, Wu et al. demonstrated 3D plasmonic core-satellite nanostructures through a DNA molecule-assisted self-assembly[26] and Solovyeva et al. used amino groups as a molecular linker for an assembly of silver NPs[24]. In addition, Lee et al. reported core-satellite gold NPs assembly with the use of dithiol molecules[27]. Linker molecules for the direct assembly of NPs enable the precise control of plasmonic hotspots, thus enhancing SERS performance.

In this study, we demonstrate a highly sensitive SERS platform based on gold NPs (AuNPs) on gold NSs (AuNSs) with a spacer layer of 1,4-benzenedimethanethiol (BDMT). Our proposed AuNP@BDMT@AuNSs SERS platform have been designed according to two distinct schemes: (1) in generating two-dimensional (2D) hotspots through large area AuNSs, and (2) in employing 3D hotspot matrix by a vertical nanogap

between AuNSs and AuNPs. In our previous work, we have discussed the morphology change of 2D AuNSs and the associated SERS enhancement according to the initial thickness of Au and the heat-treatment temperature[28]. Based on this study, the Au thin films with a thickness of ~ 4.5 nm were annealed at 550°C for 10 min to fabricate the 2D AuNSs. The BDMT uniformly adsorbed onto the surface of the AuNSs, leading to the self-assembly of nanometer-thick monolayers. The AuNP@BDMT@AuNSs were produced by immobilizing AuNPs with diameters of ~ 6–35 nm on the BDMT@AuNSs. The SERS performance of the proposed platform was evaluated using rhodamine 6G (R6G). The Raman signal of the AuNP@BDMT@AuNSs with diameter of ~ 35 nm was up to twelve times stronger than that produced by AuNSs at 100 nM of R6G. Furthermore, the proposed AuNP@BDMT@AuNSs platform was used to detect the fungicide thiram, exhibiting a limit of detection (LOD) of 13 nM.

2. Results And Discussion

Figure 1 illustrates a step-by-step fabrication procedure for AuNP@BDMT@AuNSs sensors. Au thin film is deposited on the Si surface via sputtering then subjected to thermal annealing to produce 2D AuNSs. After BDMT functionalization of the AuNS surface, AuNPs are immobilized on the BDMT@AuNSs. BDMT has a chain length of approximately 1 nm and therefore provides a vertical nanogap between the AuNSs and AuNPs[29].

Figure 2 shows the morphological, chemical, and optical characteristics of AuNPs according to the different growing steps. As shown in Fig. 2a, the diameter of the AuNPs increased from 6.3 ± 1.6 nm ($AuNP_0$), to 16.1 ± 4.5 nm ($AuNP_1$), to 34.7 ± 3.6 nm ($AuNP_2$), to 44.9 ± 4.3 nm ($AuNP_3$), to 50.2 ± 3.7 nm ($AuNP_4$) according to the different growing steps. The lower-magnification TEM images of AuNPs were depicted in Fig. S2. To demonstrate the chemical elements of the AuNPs, EDS analyses were conducted. The line-scan analysis across the AuNPs proved that Au L-edge distribution was well defined as shown in Fig. 2b. Figure 2c shows the diameter of AuNPs as an increase of the growing steps. The detailed size distributions of AuNPs were depicted in Fig. S1. The TEM image analysis of the AuNPs was performed using freeware ImageJ (ver. 1.53e) program[30]. The optical properties of the AuNP solutions measured with UV-vis spectroscopy are displayed in Fig. 2d. The absorption peak denotes the photon absorption due to the LSPR of the AuNPs, and the red-shift is observed as a successive particle growth, which is consistent with Mie theory (inset of Fig. 2d)[31].

Since the diameters of the $AuNP_3$ and the $AuNP_4$ are similar as depicted in Fig. 2c, subsequent experiments were performed except for the $AuNP_3$. Figure 3 shows the morphological and chemical properties of the AuNP@BDMT@AuNSs. Figures 3a and b present SEM images of the AuNSs and the $AuNP_2$@BDMT@AuNSs, respectively. After the thermal annealing process of the Au thin film, the larger grain size in the film were formed and as a result, 2D AuNSs were obtained. Following the immobilization of the AuNPs, the AuNPs including $AuNP_0$, $AuNP_1$, and $AuNP_2$ were rather uniformly distributed on the BDMT@AuNS surface as shown in Fig. 2b and d-f. However, the $AuNP_4$ with a diameter of ~ 50 nm was not well immobilized on the BDMT@AuNS surface (Fig. S3). In order to verify the functionalization of the

well-ordered BDMT SAMs, the surface-enhanced Raman spectrum of the BDMT@AuNSs was measured. The characteristic peak at 1586 cm^{-1} can be identified as the ring stretching mode, and those at 1218 and 1167 cm^{-1} as CH_2 wagging mode and β_{C-H} vibration mode, respectively[32,33]. Figures 3d–f show AFM images of the $AuNP_0$@BDMT@AuNSs, the $AuNP_1$@BDMT@AuNSs, and the $AuNP_2$@BDMT@AuNSs, respectively. The 3D topographic image and height profile along the line were inserted in each AFM image. From the AFM images, it can be seen that AuNPs including $AuNP_0$, $AuNP_1$, and $AuNP_2$ were well immobilized on the surface of BDMT@AuNSs.

To evaluate the SERS performance of the proposed AuNP@BDMT@AuNSs, the SERS signal of the AuNP@BDMT@AuNS sensor was measured using R6G at a range of concentrations (10^{-5} to 10^{-9} M). The R6G spectra exhibited strong peaks for vibrational bands at 611, 773, 1181, 1310, 1360, 1507, 1574, and 1648 cm^{-1}, corresponding to the Raman characteristic peaks of R6G, as shown in Fig. S4 and Table S2. Figure 4a presents the Raman spectra for the AuNSs and the AuNP@BDMT@AuNSs with differently sized AuNPs at 10 μM R6G. It is obvious that the Raman intensities of the $AuNP_2$@BDMT@AuNSs sensor are strongly enhanced, which is about eight times higher than that of the AuNSs sensor. Figure 4b shows the SERS spectra of the $AuNP_2$@BDMT@AuNSs sensor at R6G concentrations of 10^{-5} to 10^{-9} M. Figure S5a-c show the SERS spectra of the AuNSs, the $AuNP_0$@BDMT@AuNSs, and the $AuNP_1$@BDMT@AuNSs sensors at R6G concentrations of 10^{-5} to 10^{-7} M, respectively. Figure 4c presents the Raman intensity at 611 cm^{-1} as a function of the logarithmic concentration of R6G for the AuNSs, the $AuNP_0$@BDMT@AuNSs, and the $AuNP_2$@BDMT@AuNSs sensors (SERS data of the $AuNP_1$@BDMT@AuNSs sensor is separately presented in Fig. S5d for clarity). For the $AuNP_2$@BDMT@AuNSs sensor, the signal increase (ΔI) of the Raman peak at 611 cm^{-1} shows a good linear relationship with R6G logarithmic concentration C_{R6G}, which can be expressed by $Log(\Delta I) = 0.30991 Log(C_{R6G}) + 5.07964$ having an R^2 of 0.986. The SERS signal of the $AuNP_2$@BDMT@AuNSs sensor at 611 cm^{-1} increased by about 12 times compared to the AuNSs sensor at 100 nM of R6G concentration. The limit of detection (LOD) was computed according to the formula of $LOD = mean_{blank} + 1.645(SD_{blank} + SD_{analyte})$, where $mean_{blank}$ and SD_{blank} are the average and the standard deviation of (ΔI) without analyte, respectively, and $SD_{analyte}$ is the standard deviation of (ΔI) for the lowest analyte concentration measured [34]. The obtained LOD was about $10^{-10.07}$ M (~ 84 pM). To investigate the reproducibility of the $AuNP_2$@BDMT@AuNSs sensor, the Raman intensity at 611 cm^{-1} was evaluated for 11 different regions at 10 μM of R6G concentration as shown in Fig. 4d, and the relative standard deviation (RSD) was about 5.3%. Figure S6a shows the Raman intensity at 773 cm^{-1} as a function of the logarithmic concentration of R6G for the $AuNP_2$@BDMT@AuNSs sensors with an R^2 of 0.931, and the intensity distribution was depicted in Fig. S6b. The RSD was about 5.2%.

To evaluate the electric field distribution of the proposed AuNP@BDMT@AuNSs sensor, the finite element method (FEM) simulation was conducted using COMSOL Multiphysics (ver. 4.3a). Figure 5a presents the

simulation set-up. The AuNP with different diameters of 6.3 nm ($AuNP_0$), 16.1 nm ($AuNP_1$), and 34.7 nm ($AuNP_2$) and a 1 nm gap was placed on the Au thin film/Si substrate along the z-direction. The light with a wavelength of 532 nm polarized to x-axis was incident on the sensor along the z-axis. Figure 5b-d shows the electric field distributions of the $AuNP_0$, the $AuNP_1$, and the $AuNP_2$ on the Au thin film/Si substrate, respectively. It can be clearly observed that highly localized electric fields can be generated in the small gaps between the Au thin film and the AuNP. Furthermore, as the diameter of the NPs increases, the localized electric fields in the nanogap are enhanced.

To demonstrate the practical utility of our proposed sensing platform, we investigated the SERS performance of the $AuNP_2$@BDMT@AuNSs with thiram. Figure 6a shows the SERS spectra of the $AuNP_2$@BDMT@AuNSs sensor at thiram concentrations of 10^{-3} to 10^{-7} M. Figure 6b presents the signal increase (ΔI) at 558 cm^{-1} as a function of the logarithmic concentration of thiram (C_{Thiram}) described by $Log(\Delta I) = 0.1957 Log(C_{Thiram}) + 3.5109$ with the R^2 of 0.972. The LOD was found to be ~ 13 nM. Compared to the recently reported SERS substrates, this LOD value is compatible to that of other SERS substrates as depicted in Table S3. In addition, the LOD value is about 1000 times lower than the maximal residue limit of 7 ppm (~ 29 μM) in fruit [35]. These results indicate that our proposed SERS platform shows satisfactory performance, and suggests an alternative approach for highly sensitive SERS sensor.

3. Conclusions

We demonstrated the rationally designed AuNP@BDMT@AuNSs SERS platform based on the idea of employing 3D hotspots with a vertical nanogap between the AuNSs and the AuNPs after generating 2D hotspots in large area AuNSs. We evaluated the fabricated sensor using SEM, TEM, AFM, EDS, and UV-vis spectrometer. The SERS signals of R6G concentrations 10 μM to 1 nM were obtained from the AuNP@BDMT@AuNSs with differently sized AuNPs, and it was found that the SERS signal of the $AuNP_2$@BDMT@AuNSs sensor was strongly enhanced by about 12 times compared to the AuNSs sensor at 100 nM of R6G concentration. We revealed that these results were due to the strong electric fields in the nanogap between the AuNP and the AuNSs via FEM simulation. In addition, our proposed sensor was able to measure thiram up to 13 nM, showing significant potential for use in highly sensitive SERS sensors.

4. Methods

4.1. Materials

Silicon wafers were purchased from Silicon Materials Inc., USA (B-doped p-type wafer, resistivity of 1–30 Ω•cm). Rhodamine 6G, gold chloride trihydrate, 1,4-benzenedimethanethiol, n-hexane, sodium citrate, and

thiram were purchased from Sigma-Aldrich. The Au target was purchased from Thifine Inc. (2-inch diameter, purity of 99.99%). All chemicals required no further purification.

4.2. Synthesis of AuNPs with a diameter of 6–50 nm

AuNPs in aqueous suspension were obtained by seed-mediated synthesis according to the previous report[36]. Briefly, to synthesize Au seeds, 1 mL of 25 mM gold chloride trihydrate aqueous solution was injected to 150 mL of 2.2 mM sodium citrate aqueous solution at 100 ℃ under vigorous stirring. After 10 min, the color of the Au seeds changed from yellow to red-wine. For the synthesis of AuNPs up to 50 nm in diameter, the reaction suspension was allowed to cool down to 90°C. Then, 1 mL of 60 mM sodium citrate aqueous solution and 1 mL of 25 mM gold chloride trihydrate aqueous solution were added to the same vessel in consecutive order and kept for 30 min. By repeating this process four times, AuNPs with a diameter of 6–50 nm were obtained. For convenience and clarity, we denoted Au seed as $AuNP_0$, AuNPs with different diameters as $AuNP_1$ to $AuNP_4$ in the order of growing steps. Table S1 indicates the information of size and localized surface plasmon resonance (LSPR) peak wavelength in AuNPs according to growth steps. Milli-Q water was used for the preparation of all aqueous solutions.

4.3. Preparation of AuNP@BDMT@AuNSs

The 2D AuNSs were prepared following the procedure described in our previous study[28]. Briefly, Au thin films with a thickness of 4.5 nm were deposited on the Si wafers, and then thermally annealed at temperatures of 550 ℃ for 10 min. AuNP@BDMT@AuNSs sensors for SERS measurement were obtained as follows. In order to get well-ordered self-assembled monolayers (SAMs) of BDMT, AuNSs were immersed in a freshly prepared 1 mM BDMT solution of n-hexane for 30 min at 60°C and then rinsed with a fresh solution of n-hexane[37]. The as-prepared BDMT@AuNSs were subsequently washed with large volumes of water and ethanol and then immersed in an AuNP suspension having different diameters overnight at 4°C[38]. The resulting AuNP@BDMT@AuNSs were rinsed again with water before analysis.

4.4. Characterization techniques

The morphological and chemical information of the fabricated samples were characterized using scanning electron microscopy (SEM; Hitachi S-4300SE, Hitachi, Japan), transmission electron microscopy (TEM; JEM-2100F, JEOL, Japan), atomic force microscopy (AFM; NanoScope IV, Bruker, MA, USA), and Fourier transform-infrared spectrometer (FT-IR; Vertex 80V, Bruker, MA, USA). Elemental mapping was carried out using Thermo-Noran energy dispersive X-ray spectroscopy (EDS) attachment equipped with TEM (JEM-2100F). UV-vis spectrometer (Lambda 650, PerkinElmer, MA, USA) was utilized for optical characterization of the synthesized AuNPs.

4.5. SERS measurements

For monitoring of SERS behaviors to R6G, AuNSs samples and AuNP@BDMT@AuNSs samples were dipped in an aqueous solution of R6G with different concentrations ranging from 10 μM to 1 nM for 1 h, as described in our previous studies[28,39]. The samples were then rinsed in Milli-Q water and dried with a

nitrogen blow to remove the unfixed molecules. For SERS measurements of thiram, an ethanolic solution of thiram (1 mM – 100 nM) was dripped on AuNP@BDMT@AuNSs samples and then dried naturally. Raman spectra for R6G were collected on a Raman spectroscopy (LabRAM HR Evolution, HORIBA, Japan) under the conditions of an excitation wavelength of 532 nm, a laser power of 14 mW, an acquisition time of 5 s, and an accumulation of 3 in a range of 400–1800 cm^{-1}. SERS spectra for thiram were acquired at an excitation wavelength of 532 nm, a laser power of 14 mW, an acquisition time of 10 s, and an accumulation of 5 in a range of 400–1800 cm^{-1}.

Declarations

Author Contributions

DJL fabricated the sensor devices and performed the sensing experiments. DYK and DJL discussed the data and drafted the manuscript.

Declaration of Competing Interest

The authors declare no competing financial interest.

Acknowledgments

This work was supported in part by the National Research Foundation of Korea (NRF), Ministry of Education, through the Basic Science Research Program under Grant No. 2018R1A6A1A03025523, in part by the National Research Foundation of Korea (NRF) funded by the Ministry of Science and ICT under Grant No. 2019R1A2C1006814.

References

1. Lee, H. K. *et al.* Designing surface-enhanced Raman scattering (SERS) platforms beyond hotspot engineering: emerging opportunities in analyte manipulations and hybrid materials. *Chem. Soc. Rev.* **48**, 731-756, doi:10.1039/c7cs00786h (2019).
2. Ralbovsky, N. M. & Lednev, I. K. Towards development of a novel universal medical diagnostic method: Raman spectroscopy and machine learning. *Chem. Soc. Rev.* **49**, 7428-7453, doi:10.1039/d0cs01019g (2020).
3. Cardinal, M. F. *et al.* Expanding applications of SERS through versatile nanomaterials engineering. *Chem. Soc. Rev.* **46**, 3886-3903, doi:10.1039/c7cs00207f (2017).
4. Xu, M. L., Gao, Y., Han, X. X. & Zhao, B. Detection of Pesticide Residues in Food Using Surface-Enhanced Raman Spectroscopy: A Review. *J. Agric. Food Chem.* **65**, 6719-6726, doi:10.1021/acs.jafc.7b02504 (2017).
5. Liu, H., Yang, L. & Liu, J. Three-dimensional SERS hot spots for chemical sensing: Towards developing a practical analyzer. *Trac-Trends Anal. Chem.* **80**, 364-372,

doi:10.1016/j.trac.2015.08.012 (2016).

6. Huang, D. *et al.* Black phosphorus-Au filter paper-based three-dimensional SERS substrate for rapid detection of foodborne bacteria. *Appl. Surf. Sci.* **497**, 143825, doi:https://doi.org/10.1016/j.apsusc.2019.143825 (2019).
7. Liu, H. L. *et al.* Three-Dimensional and Time-Ordered Surface-Enhanced Raman Scattering Hotspot Matrix. *J. Am. Chem. Soc.* **136**, 5332-5341, doi:10.1021/ja501951v (2014).
8. Phan-Quang, G. C. *et al.* Three-Dimensional Surface-Enhanced Raman Scattering Platforms: Large-Scale Plasmonic Hotspots for New Applications in Sensing, Microreaction, and Data Storage. *Accounts Chem. Res.* **52**, 1844-1854, doi:10.1021/acs.accounts.9b00163 (2019).
9. Yang, Z. W. *et al.* 3D Hotspots Platform for Plasmon Enhanced Raman and Second Harmonic Generation Spectroscopies and Quantitative Analysis. *Adv. Opt. Mater.* **7**, doi:10.1002/adom.201901010 (2019).
10. Chen, M. *et al.* Vertically-aligned 1T/2H-MS2 (M = Mo, W) nanosheets for surface-enhanced Raman scattering with long-term stability and large-scale uniformity. *Appl. Surf. Sci.* **527**, 146769, doi:https://doi.org/10.1016/j.apsusc.2020.146769 (2020).
11. Tran, T. H. *et al.* Facile fabrication of sensitive surface enhanced Raman scattering substrate based on CuO/Ag core/shell nanowires. *Appl. Surf. Sci.* **509**, 145325, doi:https://doi.org/10.1016/j.apsusc.2020.145325 (2020).
12. Li, H. *et al.* Graphene-coated Si nanowires as substrates for surface-enhanced Raman scattering. *Appl. Surf. Sci.* **541**, 148486, doi:https://doi.org/10.1016/j.apsusc.2020.148486 (2021).
13. Li, Z. *et al.* 3D silver nanoparticles with multilayer graphene oxide as a spacer for surface enhanced Raman spectroscopy analysis. *Nanoscale* **10**, 5897-5905, doi:10.1039/c7nr09276h (2018).
14. Liu, S. Y., Tian, X. D., Zhang, Y. & Li, J. F. Quantitative Surface-Enhanced Raman Spectroscopy through the Interface-Assisted Self-Assembly of Three-Dimensional Silver Nanorod Substrates. *Anal. Chem.* **90**, 7275-7282, doi:10.1021/acs.analchem.8b00488 (2018).
15. Zhang, M. F. *et al.* Plasmonic 3D Semiconductor-Metal Nanopore Arrays for Reliable Surface-Enhanced Raman Scattering Detection and In-Site Catalytic Reaction Monitoring. *ACS Sens.* **3**, 2446-2454, doi:10.1021/acssensors.8b01023 (2018).
16. Huang, T. *et al.* A facile method to fabricate a novel 3D porous silicon/gold architecture for surface enhanced Raman scattering. *J. Alloy. Compd.* **790**, 127-133, doi:10.1016/j.jallcom.2019.03.161 (2019).
17. Wu, J. *et al.* Reusable and long-life 3D Ag nanoparticles coated Si nanowire array as sensitive SERS substrate. *Appl. Surf. Sci.* **494**, 583-590, doi:10.1016/j.apsusc.2019.07.080 (2019).
18. Gong, T. X. *et al.* Magnetic assembled 3D SERS substrate for sensitive detection of pesticide residue in soil. *Nanotechnology* **31**, doi:10.1088/1361-6528/ab72b7 (2020).
19. Han, Y., Wu, S. R., Tian, X. D. & Zhang, Y. Optimizing the SERS Performance of 3D Substrates through Tunable 3D Plasmonic Coupling toward Label-Free Liver Cancer Cell Classification. *ACS Appl. Mater. Interfaces* **12**, 28965-28974, doi:10.1021/acsami.0c04509 (2020).

20. Sun, H., Liu, H. & Wu, Y. Three-dimensional (3D) crumpled graphene-silver hybrid nanostructures on shape memory polymers for surface-enhanced Raman scattering. *Appl. Surf. Sci.* **467-468**, 554-560, doi:https://doi.org/10.1016/j.apsusc.2018.09.228 (2019).
21. Wu, J. *et al.* Reusable and long-life 3D Ag nanoparticles coated Si nanowire array as sensitive SERS substrate. *Appl. Surf. Sci.* **494**, 583-590, doi:https://doi.org/10.1016/j.apsusc.2019.07.080 (2019).
22. Caro, C., Lopez-Cartes, C., Zaderenko, P. & Mejias, J. A. Thiol-immobilized silver nanoparticle aggregate films for surface enhanced Raman scattering. *J. Raman Spectrosc.* **39**, 1162-1169, doi:10.1002/jrs.1957 (2008).
23. Bu, Y., Park, S. J. & Lee, S. W. Diamine-linked array of metal (Au, Ag) nanoparticles on glass substrates for reliable surface-enhanced Raman scattering (SERS) measurements. *Curr. Appl. Phys.* **14**, 784-789, doi:10.1016/j.cap.2014.03.008 (2014).
24. Solovyeva, E. V., Ubyivovk, E. V. & Denisova, A. S. Effect of diaminostilbene as a molecular linker on Ag nanoparticles: SERS study of aggregation and interparticle hot spots in various environments. *Colloid Surf. A-Physicochem. Eng. Asp.* **538**, 542-548, doi:10.1016/j.colsurfa.2017.11.040 (2018).
25. Tian, H. H., Li, H. B. & Fang, Y. Binary Thiol-Capped Gold Nanoparticle Monolayer Films for Quantitative Surface-Enhanced Raman Scattering Analysis. *ACS Appl. Mater. Interfaces* **11**, 16207-16213, doi:10.1021/acsami.9b02069 (2019).
26. Wu, L. A., Li, W. E., Lin, D. Z. & Chen, Y. F. Three-Dimensional SERS Substrates Formed with Plasmonic Core-Satellite Nanostructures. *Sci Rep* **7**, 13066, doi:10.1038/s41598-017-13577-9 (2017).
27. Lee, S., Kim, M. & Yoon, S. Colour and SERS patterning using core-satellite nanoassemblies. *Chem. Commun.* **55**, 1466-1469, doi:10.1039/c8cc09270b (2019).
28. Lee, D. J. & Kim, D. Y. UV Irradiation-Induced SERS Enhancement in Randomly Distributed Au Nanostructures. *Sensors (Basel)* **20**, doi:10.3390/s20143842 (2020).
29. Mahapatro, A. K., Ghosh, S. & Janes, D. B. Nanometer scale electrode separation (nanogap) using electromigration at room temperature. *IEEE Trans. Nanotechnol.* **5**, 232-236, doi:10.1109/tnano.2006.874053 (2006).
30. Schneider, C. A., Rasband, W. S. & Eliceiri, K. W. NIH Image to ImageJ: 25 years of image analysis. *Nat. Methods* **9**, 671-675, doi:10.1038/nmeth.2089 (2012).
31. Pal, S. K. G. a. T. Interparticle Coupling Effect on the Surface Plasmon Resonance of Gold Nanoparticles: From Theory to Applications. *Chem. Rev.* **107**, 4797–4862 (2007).
32. K. V. G. K. Murty, M. V., and T. Pradeep. Self-assembled Monolayers of 1,4-Benzenedimethanethiol on Polycrystalline Silver and Gold Films: An Investigation of Structure, Stability, Dynamics, and Reactivity. *Langmuir* **14**, 5446-5456 (1998).
33. Robinson, D. B., Funamura, J. R., Talin, A. A. & Anderson, R. J. Spectroscopic observation of chemical change during molecular electronics experiments. *Appl. Phys. Lett.* **90**, doi:10.1063/1.2696804 (2007).
34. Li, Y. *et al.* Fabrication of an insect-like compound-eye SERS substrate with 3D Ag nano-bowls and its application in optical sensor. *Sens. Actuator B-Chem.* **330**, doi:10.1016/j.snb.2020.129357 (2021).

35. Sun, H., Liu, H. & Wu, Y. A green, reusable SERS film with high sensitivity for in-situ detection of thiram in apple juice. *Appl. Surf. Sci.* **416**, 704-709, doi:10.1016/j.apsusc.2017.04.159 (2017).
36. Bastus, N. G., Comenge, J. & Puntes, V. Kinetically controlled seeded growth synthesis of citrate-stabilized gold nanoparticles of up to 200 nm: size focusing versus Ostwald ripening. *Langmuir* **27**, 11098-11105, doi:10.1021/la201938u (2011).
37. Hamoudi, H. *et al.* Self-assembly of 1,4-benzenedimethanethiol self-assembled monolayers on gold. *Langmuir* **26**, 7242-7247, doi:10.1021/la904317b (2010).
38. Merli, D. *et al.* A gold nanoparticle chemically modified gold electrode for the determination of surfactants. *RSC Adv.* **6**, 106500-106507, doi:10.1039/c6ra22223d (2016).
39. Lee, D. J. & Kim, D. Y. Hydrophobic Paper-Based SERS Sensor Using Gold Nanoparticles Arranged on Graphene Oxide Flakes. *Sensors (Basel)* **19**, doi:10.3390/s19245471 (2019).

Figures

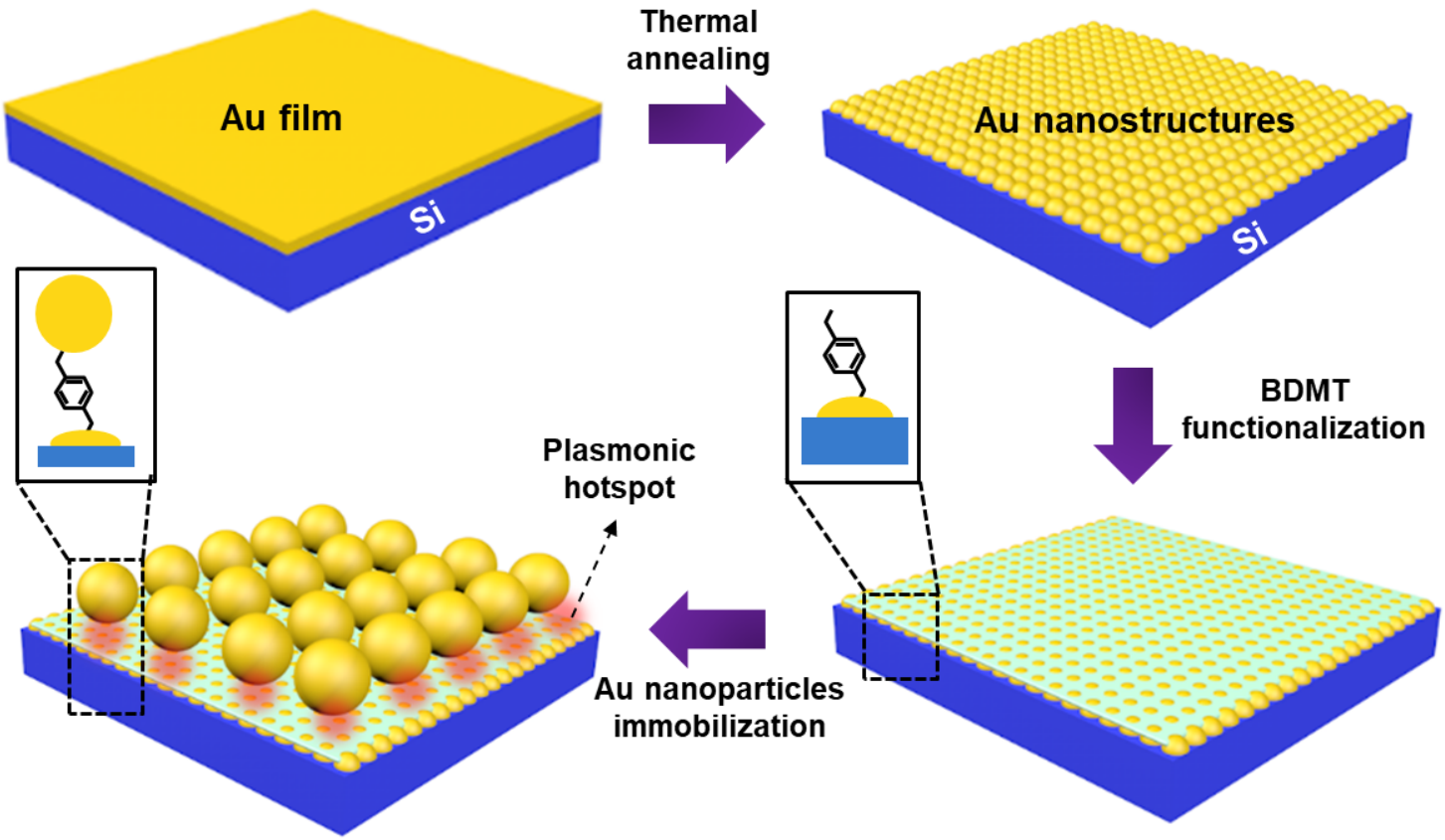

Figure 1

Schematic diagram of the fabrication process for AuNP@BDMT@AuNSs. AuNSs are made by thermal annealing of Au thin film, and AuNP@BDMT@AuNSs are fabricated through immobilization of AuNPs on the BDMT@AuNSs.

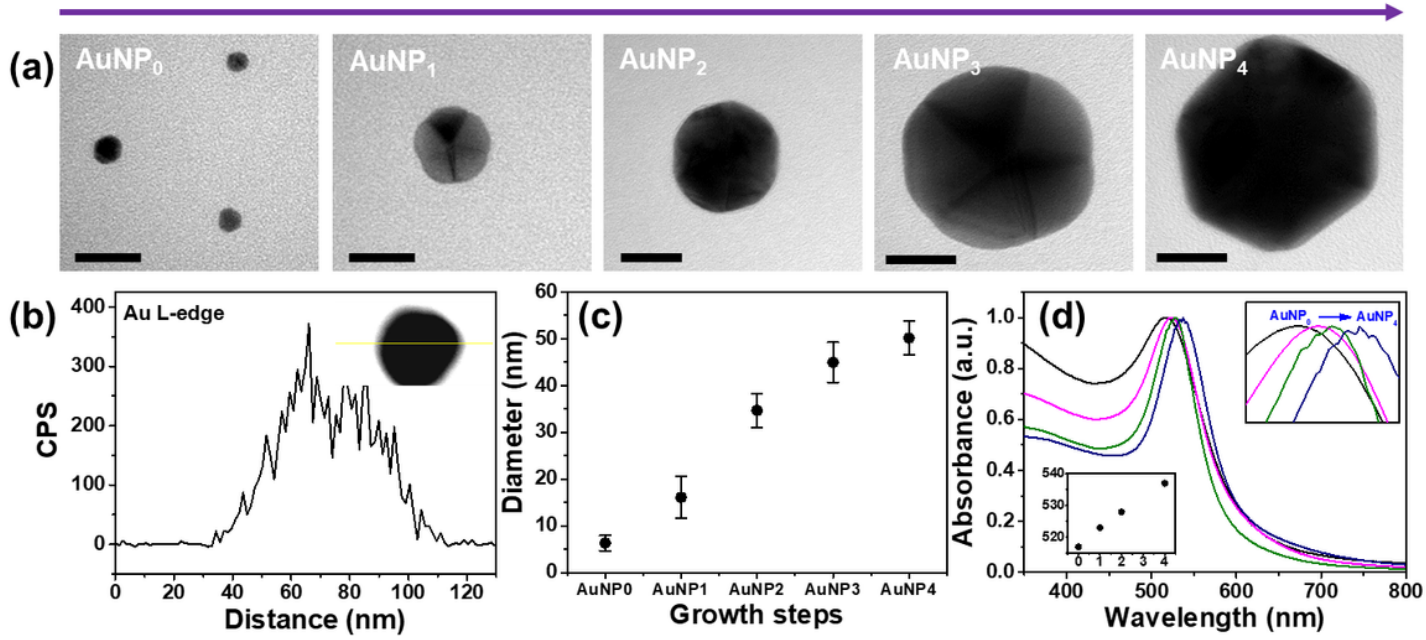

Figure 2

Morphological, chemical, and optical characteristics of the AuNPs. (a) TEM images of AuNPs according to the different growing steps. The scale bar is 20 nm. (b) EDS line-scan analysis of Au L-edge distribution across the AuNPs. Size distribution (c) and UV-vis spectra of AuNP0 to AuNP4.

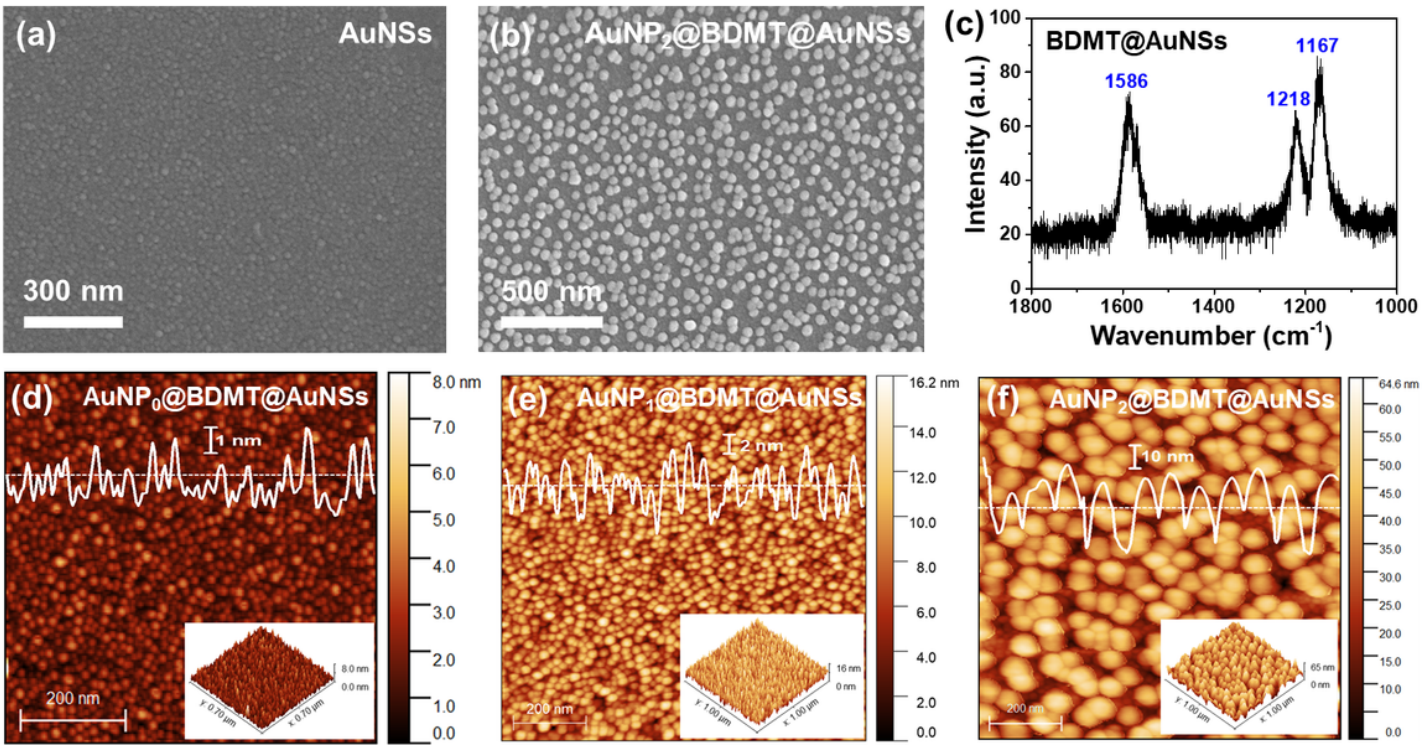

Figure 3

Morphological and chemical properties of the AuNP@BDMT@AuNSs. (a) and (b) SEM images of the AuNSs and the AuNP2@BDMT@AuNSs, respectively. (c) Raman spectrum of the BDMT@AuNSs. The

characteristic peaks of 1586, 1218, and 1167 cm-1 corresponds to ring stretching, CH2 wagging, and βC-H vibration modes of the BDMT SAMs, respectively. (d)–(f) AFM images of the AuNP@BDMT@AuNSs with differently sized AuNPs. The white line profile inserted in each AFM image represents the height information along the line.

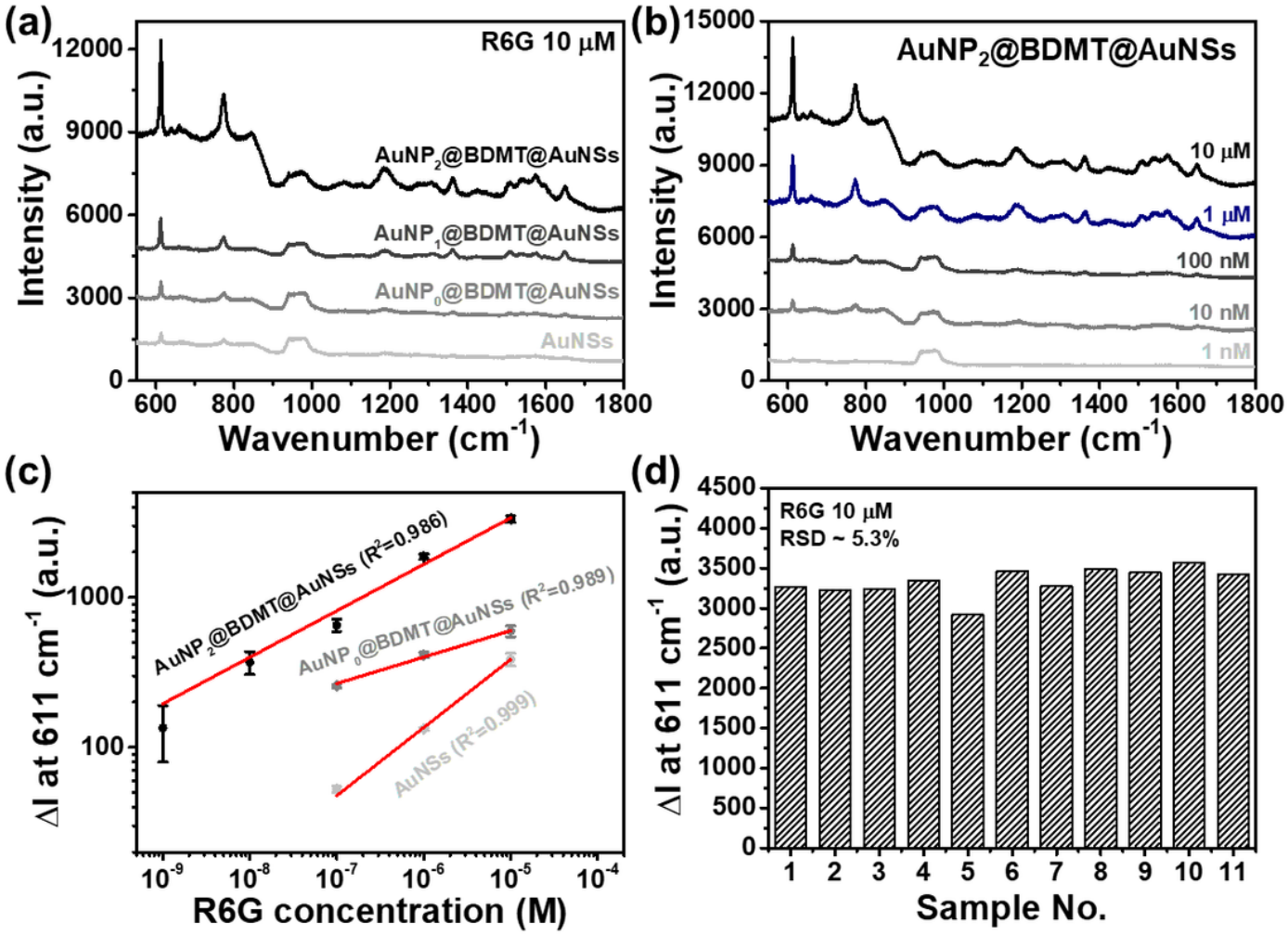

Figure 4

SERS performance of the AuNP@BDMT@AuNSs for R6G. (a) Raman spectra for the AuNSs and the AuNP@BDMT@AuNSs with differently sized AuNPs at 10 μM of R6G concentration. The Raman signal of the AuNP2@BDMT@AuNSs sensor is about eight times higher than that of AuNSs sensor. (b) SERS spectra of the AuNP2@BDMT@AuNSs sensor at R6G concentrations of 10-5 to 10-9 M. (c) Raman intensity at 611 cm-1 as a function of the logarithmic concentration of R6G for the AuNSs, the AuNP0@BDMT@AuNSs, and the AuNP2@BDMT@AuNSs sensor. (d) Intensity distribution at 611 cm-1 was evaluated for 11 different regions at 10 μM of R6G concentration for the AuNP2@BDMT@AuNSs sensor.

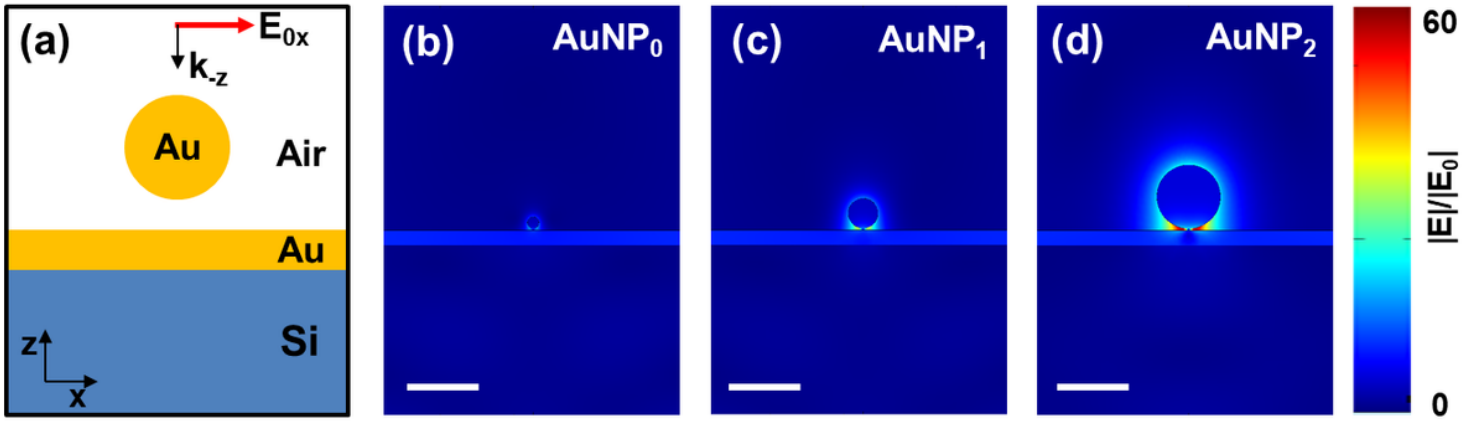

Figure 5

FEM simulation of an AuNP on an Au surface with a vertical nanogap. (a) Simulation set-up of the proposed AuNP@BDMT@AuNSs. (b-d) Electric field distributions of the AuNP0, the AuNP1, and the AuNP2 on the Au thin film/Si substrate, respectively. The scale bar is 30 nm.

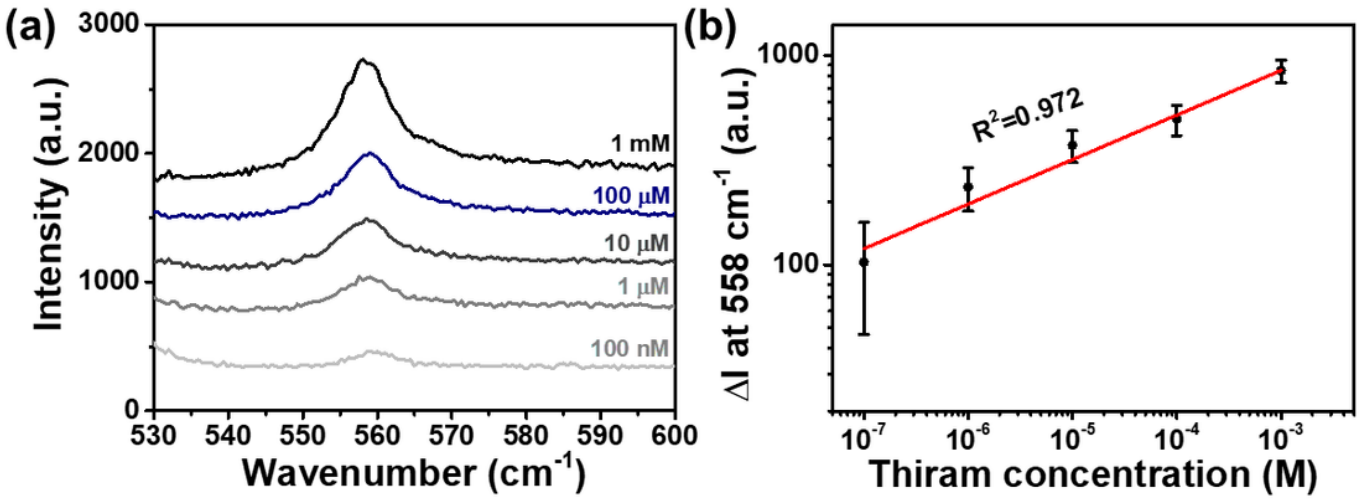

Figure 6

SERS enhancement of the AuNP2@BDMT@AuNSs for thiram. (a) SERS spectra of the AuNP2@BDMT@AuNSs sensor at thiram concentrations of 10-5 to 10-7 M. (b) Raman intensity at 558 cm-1 as a function of the logarithmic concentration of thiram.

Supplementary Files

This is a list of supplementary files associated with this preprint. Click to download.

- SupportingInformationSR.pdf